antioxidants

MDPI

Article

New Megastigmane and Polyphenolic Components of Henna Leaves and Their Tumor-Specific Cytotoxicity on Human Oral Squamous Carcinoma Cell Lines

Mohamed A. A. Orabi [1,*], Esam A. Orabi [2,*], Ahmed Abdullah Al Awadh [3], Mohammed Merae Alshahrani [3], Basel A. Abdel-Wahab [4], Hiroshi Sakagami [5] and Tsutomu Hatano [6]

1 Department of Pharmacognosy, College of Pharmacy, Najran University, Najran 66454, Saudi Arabia
2 Department of Chemistry and Biochemistry, Concordia University, 7141 Sherbrooke Street West, Montréal, QC H4B 1R6, Canada
3 Department of Clinical Laboratory Sciences, Faculty of Applied Medical Sciences, Najran University, Najran 66454, Saudi Arabia; aaalawadh@nu.edu.sa (A.A.A.A.); mmalshahrani@nu.edu.sa (M.M.A.)
4 Department of Pharmacology, College of Pharmacy, Najran University, Najran 64462, Saudi Arabia; babdelnaem@nu.edu.sa
5 Meikai University Research Institute of Odontology (M-RIO), 1-1 Keyakidai, Saitama 350-0283, Japan; sakagami@dent.meikai.ac.jp
6 Graduate School of Medicine, Dentistry and Pharmaceutical Sciences, Okayama University, Tsushima, Okayama 700-8530, Japan; hatano-t@cc.okayama-u.ac.jp
* Correspondence: mohamedorabi@azhar.edu.eg (M.A.A.O.); e_orabi@live.concordia.ca (E.A.O.)

Abstract: Polyphenols have a variety of phenolic hydroxyl and carbonyl functionalities that enable them to scavenge many oxidants, thereby preserving the human redox balance and preventing a number of oxidative stress-related chronic degenerative diseases. In our ongoing investigation of polyphenol-rich plants in search of novel molecules, we resumed the investigation of *Lawsonia inermis* L. (Lythraceae) or henna, a popular ancient plant with aesthetic and therapeutic benefits. The leaves' 70% *aq* acetone extract was fractionated on a Diaion HP-20 column with different ratios of H_2O/an organic solvent. Multistep gel chromatographic fractionation and HPLC purification of the Diaion 75% *aq* MeOH and MeOH fractions led to a new compound (**1**) along with tannin-related metabolites, benzoic acid (**2**), benzyl 6′-*O*-galloyl-*β*-D-glucopyranoside (**3**), and ellagic acid (**4**), which are first isolated from henna. Repeating the procedures on the Diaion 50% *aq* MeOH eluate led to the first-time isolation of two *O*-glucosidic ellagitannins, heterophylliin A (**5**), and gemin D (**6**), in addition to four known *C*-glycosidic ellagitannins, lythracin D (**7**), pedunculagin (**8**), flosin B (**9**), and lagerstroemin (**10**). The compound structures were determined through intensive spectroscopic investigations, including HRESIMS, 1D (^{1}H and ^{13}C) and 2D (^{1}H–^{1}H COSY, HSQC, HMBC, and NOESY) NMR, UV, $[\alpha]_D$, and CD experiments. The new structure of **1** was determined to be a megastigmane glucoside gallate; its biosynthesis from gallic acid and a *β*-ionone, a degradative product of the common metabolite *β*-carotin, was highlighted. Cytotoxicity investigations of the abundant ellagitannins revealed that lythracin D2 (**7**) and pedunculagin (**8**) are obviously more cytotoxic (tumor specificity = 2.3 and 2.8, respectively) toward oral squamous cell carcinoma cell lines (HSC-2, HSC-4, and Ca9-22) than normal human oral cells (HGF, HPC, and HPLF). In summary, *Lawsonia inermis* is a rich source of anti-oral cancer ellagitannins. Also, the several discovered polyphenolics highlighted here emphasize the numerous biological benefits of henna and encourage further clinical studies to profit from their antioxidant properties against oxidative stress-related disorders.

Keywords: lythraceae; henna; *Lawsonia inermis*; megastigmane; polyphenols; oral cancer; cytotoxicity; antioxidants; molecular docking

Citation: Orabi, M.A.A.; Orabi, E.A.; Awadh, A.A.A.; Alshahrani, M.M.; Abdel-Wahab, B.A.; Sakagami, H.; Hatano, T. New Megastigmane and Polyphenolic Components of Henna Leaves and Their Tumor-Specific Cytotoxicity on Human Oral Squamous Carcinoma Cell Lines. *Antioxidants* **2023**, *12*, 1951. https://doi.org/10.3390/antiox12111951

Academic Editors: Susana M. Cardoso, Dulcineia Ferreira Wessel and Marcelo D. Catarino

Received: 25 September 2023
Revised: 29 October 2023
Accepted: 30 October 2023
Published: 1 November 2023

1. Introduction

The study of polyphenolic phytochemicals for drug development has grown significantly in recent decades. Polyphenols can participate in redox activities that are required for various metabolic events due to their many phenolic hydroxyl and carbonyl functionalities. As a result, they can prevent a variety of chronic degenerative illnesses and maintain human homeostasis [1]. The plant polyphenols are widely varied in their chemical structures among different families of the plant kingdom or within the same family, and how they interact—whether specifically or not—with biomolecules relies heavily on both their own physicochemical properties and those of the biomolecule partners [2].

In our ongoing investigation of polyphenol-rich plants in search of novel molecules, we resumed the investigation of *Lawsonia inermis* L. (Syn. *L. alba*) (Lythraceae), or henna, as one with special healing qualities in ancient medicines. Henna, which refers to the dye prepared from the plant, is naturally grown from Northeast Africa to India and has been extensively used for centuries in the Middle East, Far East, and Northern Africa as a cosmetic dye for nails, hands, hair, and textiles. It has also been used to tackle skin issues, headaches, jaundice, amebiasis, and spleen enlargement [3–5]. The plant extracts and purified constituents of henna account for a variety of activities, including anti-Alzheimer's, antioxidant, hepatoprotective, immunomodulatory, cytotoxic, antibacterial, antifungal, analgesic, anti-inflammatory and antipyretic, hypotensive, sedative, and anticancer effects (Figure 1) [3,6–10]. Oral administration of *L. inermis* leaf extracts significantly suppressed the growth of B16F10 tumors in mice with an increased tumor necrosis area and increased infiltration of mononuclear cells at the site of the tumor [11]. The in vivo antitumor effect of *L. inermis* extracts was directly linked to the enhanced antioxidant activity, which is the main quality of plant polyphenols [11]. In our preceding articles on henna leaf extracts, we demonstrated the occurrence of ellagitannins in abundance and reported on their anticholinesterase and cytotoxic activities [12,13]. The structure and molecular weight of ellagitannins determine their inhibitory capacities against the initiation and spread of tumors, which are subsequently influenced by their antioxidant and binding qualities [12].

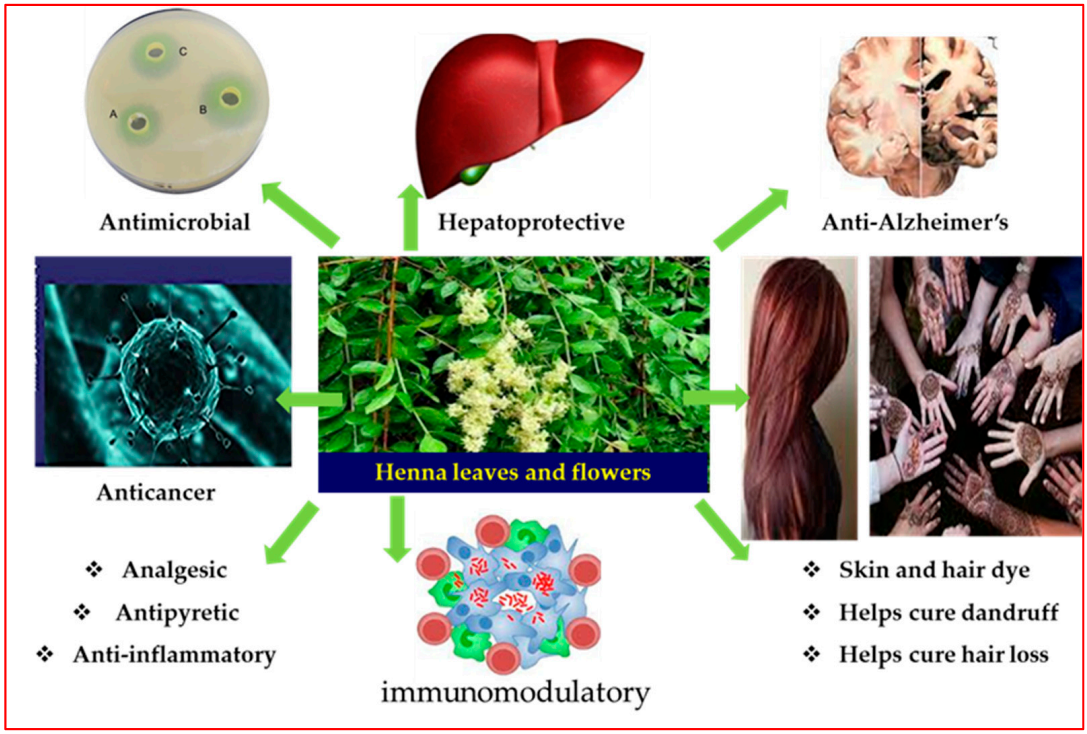

Figure 1. Summary of major bioactivities of henna metabolites.

The isolation–identification procedures of therapeutic metabolites is a potential research focus for the next steps of our studies. Further phytochemical investigations of different fractions of the *L. inermis* leaf extract may lead to the exploration of novel constituents that could explain the extract's various biological areas of significance.

In this study, a chromatographic investigation of phenolic-rich fractions of the henna leaf extract led to the isolation of a new megastigmane, lawsoiononoside (**1**), together with the first-time isolation of tannin-related phenolics, benzyl 6′-O-galloyl-*β*-D-glucopyranoside (**2**), benzoic acid (**3**), and ellagic acid (**4**), whereas an extensive investigation of the tannin-rich fractions led to two glucopyranose-type ellagitannins (**5** and **6**) in addition to four known *C*-glycosidic ones (**7**–**10**). The cytotoxicity of the abundant ellagitannins (**8**–**10**) to various human oral cancer and normal cell lines was examined in the present study.

2. Materials and Methods

2.1. General Experimental Procedures

Electronic circular dichroism (ECD) and ultraviolet (UV) spectra were recorded on JASCO J-720W (JASCO, Tokyo, Japan) and JASCO V-530 (JASCO, Tokyo, Japan) spectrophotometers, respectively. The optical rotation was measured on a JASCO DIP-1000 (JASCO, Tokyo, Japan) digital polarimeter. High-resolution electrospray ionization mass (HRESIMS) spectra were acquired on a Micromass AutoSpec OA-TOF (Manchester, UK) spectrometer. Samples in H_2O/MeOH (1:1, *v*/*v*) + 0.1% NH_4OAc were infused into the ESI source at a flow rate of 20 μL/min. The NMR spectra were acquired on a Varian INOVA AS600 (Varian, Palo Alto, CA, USA) instrument (600 MHz for ^1H and 151 MHz for ^{13}C). Chemical shifts are given in δ (ppm) relative to that of the solvent signal [$(CH_3)_2CO$-d_6 (δ_H 2.04; δ_C 29.8)] on the tetramethylsilane (TMS) scale.

The fractionation and purification procedures were monitored by normal-phase (NP) and reversed-phase (RP) high-performance liquid chromatography (HPLC). The NP-HPLC analyses were performed on a YMC-Pack SIL A-003 (YMC, Kyoto, Japan) column (4.6 × 250 mm) using a mobile phase composed of *n*-hexane/MeOH/tetrahydrofuran/formic acid (55:33:11:1, *v*/*v*) + oxalic acid (450 mg/L). The flow rate was adjusted at 1.5 mL/min at room temperature, and eluates were monitored using a UV detector at 280 nm. The RPHPLC analyses were performed on a YMC-Pack ODS-A A-302 column (4.6 × 150 mm) (YMC, Japan) with a 0.01 M H_3PO_4/0.01 M KH_2PO_4/MeOH (1:1:0.5, *v*/*v*) mobile phase at a flow rate of 1.0 mL/min at 40 °C and UV detection at 280 nm. Preparative RP-HPLC was performed at 40 °C on a YMC-Pack ODS-A A-324 column (10 × 300 mm) at a flow rate of 2.0 mL/min and the same UV detector. The composition of the mobile phases used in the RPHPLC purifications are specified in the extraction and isolation procedures below. The gels used for column chromatography were Diaion HP-20 (Mitsubishi Chemical, Tokyo, Japan), MCI-gel CHP-20P, Toyopearl HW-40C (TOSOH, Tokyo, Japan), and Sephadex LH-20 (GE Healthcare Bio-Science AB, Sweden).

2.2. Plant Material

L. inermis leaves were obtained from mature trees around the court collections, Assiut city, Egypt. The plant was authenticated by Professor Salah M. I. El-Najjar, Department of Botany, Assiut University, Egypt. A specimen numbered Li-05013 was kept in the department of Pharmacognosy, Al-Azhar University, Assiut, Egypt.

2.3. Extraction and Isolation

Dry *L. inermis* powdered leaves (200 g) were defatted by repeated steeping in *n*-hexane for 1.5 L × 3 consecutive days. The defatted marc was squeezed well and left to dry from the *n*-hexane, and then it was homogenized in 70% *aq* acetone (4 × 1.5 L). The solvent was dried off under vacuum, and the solute was coarsely fractionated on a Diaion HP-20 column (10 × 81 cm, i.d.) with H_2O (3 L), 50% *aq* MeOH (4.5 L), 75% *aq* MeOH (3 L), MeOH (3 L), and 70% *aq* $(CH_3)_2CO$ (2 L), successively. Each eluate was dried at 40 °C under vacuum to afford the dry fraction weights of 37.7 g, 17.24 g, 1.6 g, 0.43 g, and 0.066 g,

respectively. The different eluates, except for the 50% *aq* MeOH eluate, revealed plant metabolites with t_R < 4 min in the NP-HPLC chromatograms [14].

The MeOH fraction (0.43 g) from the Diaion column was dissolved in MeOH. The MeOH-soluble part was vacuum-dried (115 mg) and then dissolved in a 15% *aq* MeOH. The soluble part was chromatographed on an ODS column (2.2 × 40 cm, i.d.) with *aq* MeOH (15%, 25%, and 35%) and MeOH. The 25% and 35% *aq* MeOH eluates afforded benzoic acid (**3**, 10 mg) and ellagic acid (**4**, 14 mg), respectively.

The Diaion 75% *aq* MeOH fraction (1.6 g) was dissolved in H_2O, and the H_2O-soluble part was applied to an MCI-gel CHP-20P column (1.1 × 37 cm, i.d.) and eluted with H_2O and H_2O/MeOH (9:1, 8:2, 7:3, 6:4, 5:5, 0:10, *v*/*v*). The H_2O/MeOH (6:4, *v*/*v*) eluate (210 mg) was further worked on an ODS column (2.2 × 40 cm, i.d.), and eluted with H_2O and H_2O/MeOH (9:1, 8:2, 7.5:2.5, and 5:5, *v*/*v*), collecting 700 drops/fraction. Fractions 58–65 (7.3 mg) from the H_2O/MeOH (8:2, *v*/*v*) eluate were further purified using preparative RP-HPLC with [H_2O/CH_3CN (8:2, *v*/*v*) + 1% CH_3COOH)] and yielded pure lawsoiononoside (**1**, 1.3 mg) and benzyl 6′-*O*-galloyl-β-D-glucopyranoside (**2**, 1.8 mg).

A part (10 g) of the diaion 50% *aq* MeOH fraction was further fractionated on a Toyopearl HW-40C column (2.2 × 72 cm) eluted with *aq* EtOH (50%, 60%, and 70%), 70% *aq* EtOH/70% *aq* $CH_3)_2CO$ gradients (9:1, 8:2, 7:3, 6:4, and 5:5, *v*/*v*), and finally 70% *aq* $CH_3)_2CO$, successively. The Toyopearl factions (1000 drops/fraction) were analyzed via NP-HPLC and/or RPHPLC, and the fractions with similar chromatographic profiles were combined.

Toyopearl fractions T90–T105 (35 mg), eluted with 50% *aq* EtOH, were chromatographed on an MCI-gel CHP-20P column (1.1 × 37 cm) using H_2O and then H_2O/MeOH (9:1, 8.5:1.5, 8:2, 7.5:2.5, 7:3, 6.5:3.5, 5:5, and 0:10) as mobile phases. The early eluate with H_2O/MeOH (8:2, *v*/*v*) afforded crude (40 mg) and pure gemin D (**6**, 3.5 mg). Toyopearl fractions T105–T124 (87 mg), eluted with 50% *aq* EtOH, were purified on an MCI-gel CHP-20P column (1.1 × 37 cm) with the same elution mode. The H_2O/MeOH (8.5:1.5, *v*/*v*) eluate afforded pedunculagin (**8**, 22.9 mg), while the H_2O/MeOH (6.5:3.5, *v*/*v*) eluate afforded heterophylliin A (**5**, 2.6 mg). Using the same MCI-gel CHP-20P column and eluants, the Toyopearl fractions T156–T183 (259 mg) afforded flosin B (**9**, 8.1 mg) in the early eluate with H_2O/MeOH (7.5:2.5, *v*/*v*). The H_2O-insoluble part of the Toyopearl fractions T240–T347 (347 mg) afforded lagerstroemin (**10**, 46.8 mg). The H_2O-soluble part was then chromatographed using the same MCI-gel CHP-20P column (1.1 × 37 cm) with the same elution profile. The early eluate with H_2O/MeOH (8.5:1.5, *v*/*v*) afforded lythracin D (**8**, 13.4 mg).

2.4. Spectroscopic Data of Isolated Compounds

- Lawsoiononoside (**1**): Colorless gummy solid, $[\alpha]^{27}_D$: −125.6 (*c* 1.0, MeOH); UV λ_{max} (MeOH) nm (log ε): 221 (4.2), 240 (4.0), 277 (3.6); ECD (MeOH) [θ] (nm): $+2.0 \times 10^3$ (222), -2.1×10^3 (332), $+0.3 \times 10^3$ (376); NMR data; HRESIMS *m*/*z* 563.2072 $[M + Na]^+$ (calcd for $C_{26}H_{36}O_{12}Na$, 563.2099) and *m*/*z* 539.2128 $[M - H]^-$ (calcd for $C_{26}H_{35}O_{12}$, 539.2134).
- Benzoic acid (**2**): Colorless crystalline solid, ^{1}H NMR (600 MHz, DMSO-d_6) δ_H 12.9 (br.s, 1H, COOH), 7.95 (dd, *J* = 1.8, 7.2 Hz, 2H, H-2/H-6), 7.62 (tt, *J* = 1.8, 7.2 Hz, 1H, H-4), and 7.50 (dd, *J* = 7.2, 7.2 Hz, 2H, H-3/H-5); ^{13}C NMR (151 MHz, DMSO-d_6) δ_C 167.23 (C-7), 132.89 (C-4), 130.7 (C-1), 129.2 (C-2/C-6), 128.5 (C-3/C-5) [15].
- Benzyl 6′-*O*-galloyl-β-D-glucopyranoside (**4**): White amorphous powder, ^{1}H NMR (600 MHz, Me_2CO-d_6: D_2O; 9:1): δ_H 7.33 (2H, dd, *J* = 1.2, 7.8 Hz, H-2/H-6), 7.26 (2H, dt, *J* = 1.2, 7.8 Hz, H-3/H-5), 7.20 (1H, dt, *J* = 1.2, 7.8 Hz, H-4), 7.13 (2H, s, gal H-2″/H-6″), 4.79, 4.59 (each 1H, d, *J* = 12 Hz, H-7), 4.55 [1H, dd, *J* = 1.8, 12 Hz, glc H-6′], 4.39 (1H, d, *J* = 8.4 Hz, glc H-1′), 4.34 (1H, dd, *J* = 6.6, 12.6 Hz, glc H-6′), 3.29 (1H, dd, *J* = 8, 9 Hz, glc H-2′), 3.44 (1H, t, *J* = 9 Hz, glc H-3′), 3.44 (1H, t, *J* = 9 Hz, glc H-4′), 3.57 (1H, ddd, *J* = 1.8, 6, 9 Hz, glc H-5′); ^{13}C NMR (151 MHz, Me_2CO-d_6: D_2O; 9:1) δ_C: 167.2 (gal C-7″), 146.0 (2C, gal C-3″/C-5″), 138.6 (gal C-4″), 137.7 (C-1), 128.9 (2C,

C-3/C-5), 128.8 (2C, C-2/C-6), 128.2 (C-4), 121.0 (gal C-1″), 109.7 (2C, gal C-2″/C-6″), 102.7 (glc C-1″), 77.5 (glc C-3′), 74.8 (glc C-5′), 74.5 (glc C-2′), 71.2 (glc C-4′), 70.9 (C-7′), 64.5 (glc C-6′); ESIMS m/z 421 $[M - H]^-$ [16].

- Ellagic acid (**4**): Pale-yellow amorphous powder, ^{1}H NMR (600 MHz, DMSO-d_6) δ_H 10.69 (br. s, OH), 7.50 (s, 2H, H-2/H-2′); ^{13}C NMR (151MHz, DMSO-d_6) δ_C: 159.5 (2C, C-7, C-7′), 148.5 (2C, C-4/C-4′), 140.00 (2C, C-2/C-2′), 136.8 (2C, C-3/C-3′), 112.7 (2C, C-6/C-6′), 110.6 (2C, C-5/C-5′), 108.0 (2C, C-1/C-1′); ESIMS m/z 301 $[M - H]^-$ [17].
- Heterophylliin A (**5**): Off-white amorphous powder; ^{1}H NMR (600 MHz, $(CH_3)_2CO$-d_6: D_2O; 9:1) δ_H 7.23, 7.03 (each 2H, s, gal H-2/H-6), 6.61, 6.48 (each 1H, s, HHDP H-3, H-3′), 6.39 (1H, d, J = 4.2 Hz, glc H-1), 5.64 (1H, t, J = 10.2 Hz, glc H-3), 5.22 (1H, dd, J = 13.2, 6.6 Hz, glc H-6), 5.05 (1H, t, J = 10.2 Hz, glc H-4), 4.55 (1H, br. dd, J = 6.6, 10.2 Hz, glc H-5), 4.20 (1H, dd, J = 4.2, 10.2 Hz, glc H-2), Hz, 3.75 (1H, br. d, J = 13.2 Hz, glc H-6) [18].
- Gemin D (**6**): Off-white amorphous powder, ^{1}H NMR (600 MHz, $(CH_3)_2CO$-d_6: D_2O; 9:1) (α- and β-anomers) δ_H: 7.01, 7.00 (each s, 2H in total, gal H-2/H-6), 6.59, 6.58 (each s, 1H in total, HHDP H-3), 6.44, 6.43 (each s, 1H in total, HHDP H-3′), 5.46, 5.28 (1H in total, each t, J = 10.2 Hz, glc H-3α, β), 5.24 (1/2H, d, J = 4.2 Hz, glc H-1α), 5.21, 5.18 (1H in total, each dd, J = 6.6, 10.2 Hz, H-6α, β), 4.95, 4.92 (1H in total, each t, J = 10.2 Hz, H-4α, β), 4.72 (1/2H, d, J = 7.2 Hz, H-1β), 4.52, 4.06 (1H in total, each ddd, J = 1.2, 6.6, 10.2 Hz, H-5α, β), 3.81 (1/2H, dd, J = 4.2, 10.2 Hz, H-2α), 3.78, 3.71 (1H in total, each dd, J = 1.2, 13.2 Hz, H-6α, β), 3.57 (1/2H, dd, J = 7.2, 10.2 Hz, H-2β) [19].
- Lythracin D (**7**): Off-white amorphous powder, ^{1}H NMR (600 MHz, $(CH_3)_2CO$-d_6: D_2O; 9:1) δ_H: 7.08, 6.57, 6.60 (each 1H, s, valoneoyl-H), 6.73, (1H, s, flavogallonyl-H), 6.91, 6.61, 6.54 (each 1H, s, HHDP-H); 4.90 (1H, d, J = 1.8 Hz, glc-1 H-1), 4.81 (1H, t, J = 1.8 Hz, glc-1 H-2), 5.08 (1H, t, J = 1.8 Hz, glc-1 H-3), 5.62 (1H, dd, J = 1.8, 8.4 Hz, glc-1 H-4), 5.38 (1H, ddd, J = 1.2, 4.8, 9.6 Hz, glc-1 H-5), 4.92 (1H, dd, J = 2.4, 12.6 Hz, glc H-6), 3.73 (1H, d, J = 12.6 Hz, glc-1 H-6), 4.75 (1H, d, J = 1.8 Hz, glc-2 H-1), 5.01 (1H, t, J = 1.8 Hz, glc H-2), 4.50 (1H, dd, J = 1.2, 6.6 Hz, glc-2 H-3), 5.12 (1H, t, J = 7.2 Hz, glc-2 H-4), 5.55 (1H, dt, J = 1.8, 7.2 Hz, glc-2 H-5), 4.93 (1H, dd, J = 2.4, 12.6 Hz, glc-2 H-6), 3.89 (1H, d, J = 12.6 Hz, glc-2 H-6) [13].
- Pedunculagin (**8**): Off-white amorphous powder, ^{1}H NMR [600 MHz, $(CH_3)_2CO$-d_6: D_2O; 9:1] (α and β-anomer mixture) δ_H: 6.64, 6.63, 6,60, 6.59, 6.54, 6.50, 6.323, 6.321 (each, s, 4H in total, HHDP-H), 5.43 (1/H, t, J = 9.6 Hz, glc H-3α), 5.41 (1/2H, d, J = 3.6 Hz, glc H-1α), 5.24, 5.20 (1H in total, each dd, J = 6.6, 12.6 Hz, glc H-6 α, β), 5.19 (1/2H, t, J = 9.6 Hz, glc H-3β), 5.033, 5.027 (1H in total, each t, J = 9.6Hz, glc H-4 α, β), 5.01 (1/2H, d, J = 7.8 Hz, glc H-1β), 4.82 (1/2H, dd, J = 7.8, 9.6 Hz, glc H-2β), 4.57, 4.18 (1H in total, each ddd, J = 1.8, 6.6, 9.6 Hz, glc H-5α, β), 3.83, 3.76 (each 1H, dd, J = 1.2, 12.6 Hz, glc H-6α, β] [13].
- Flosin B (**9**): Off-white amorphous powder, ^{1}H NMR [600 MHz, $(CH_3)_2CO$-d_6: D_2O; 9:1] δ_H: 7.57, 7.16, 7.12 (each 1H, s, valoneoyl dilactone-H), 6.84, 6.45, 6.35 (each 1H, s, HHDP-H), 5.51 (1H, dd, J = 2.4, 8.4 Hz, glc H-4), 5.18 (1H, br.dd, J = 4.8, 9.6 Hz, glc H-5), 4.98 (1H, t, J = 2.4 Hz, glc H-3), 4.97 (1H, d, J = 2.4 Hz, glc H-1), 4.78 (1H, t, J = 1.8 Hz, glc H-2), 4.70 (1H, dd, J = 3.6, 13.2 Hz, glc H-6), 3.71 (1H, d, J = 12.6 Hz, glc H-6) [13].
- Lagerstroemin (**10**): Off-white amorphous powder, ^{1}H NMR [600 MHz, $(CH_3)_2CO$-d_6: D_2O; 9:1] δ_H: 7.57, 7.16, 7.13 (each 1H, s, valoneoyl dilactone-H), 6.76, 6.53, 6.36 (each 1H, s, HHDP-H), 5.57 (1H, d, J = 4.8 Hz, glc H-1), 5.38 (1H, t, J = 1.8 Hz, glc H-3), 5.36 (1H, dd, J = 2.4, 9 Hz, glc H-5), 5.19 (1H, dd, J = 3.6, 9 Hz, glc H-4), 4.64 (1H, dd, J = 3, 12.6, glc H-6), 4.61 (1H, dd, J = 1.8, 4.8, glc H-2), 3.72 (1H, d, J = 12.6, glc H-6) [13].

2.5. Cytotoxicity

2.5.1. Cell Culture

Four oral squamous cell carcinoma (OSCC) cell lines (Ca9-22 derived from gingiva; HSC-2, HSC-3, and HSC-4 derived from tongue) were purchased from RIKEN Cell Bank,

Tsukuba, Japan. Three human oral mesenchymal cell types, [gingival fibroblast (HGF), periodontal ligament fibroblast (HPLF), and pulp cell (HPC)], at 10–18 population doubling level were cultured at 37 °C in DMEM supplemented with 10% heat-inactivated FBS (56 °C, 30 min), 100 U/mL penicillin G, and 100 μg/mL streptomycin sulfate under a humidified 5% CO_2 atmosphere [20].

It is best to use human epithelial normal oral cells, if possible, for the comparison of drug-sensitivity with OSCC. However, when two human normal epithelial cells (human oral keratinocyte (HOK) and human gingival epithelium progenitors (HGEP)) were cultured in the regular culture medium (DMEM +10% heat-inactivated FBS), their growths were immediately stopped. Therefore, in order to maintain their growth, it was necessary to culture them in the commercially available special media supplemented with growth factors. However, we found that such stimulated epithelial (HOK/HGEP) cells began to grow like cancer cell lines, showing extremely high sensitivity against many anticancer drugs (camptothecin, SN-38 (active principal of irinotecan), doxorubicin, daunorubicin, etoposide, mitomycin C, 5-FU, docetaxel, melphalan and even molecular-targeted drug, gefitinib) [21]. At present, normal human epithelial cells cannot be used as controls. Based on this background, we used three normal oral mesenchymal cells (HGF, HPLF, HPC) in the present study. Further studies are necessary to establish the optimization of the culture condition of normal epithelial cells for use as controls and the composition of HPC cells.

2.5.2. Cytotoxicity Assay

Cells were detached from the culture dishes using 0.25% trypsin, inoculated at 2×10^3 cells per 100 μL in a 96-microwell plate and incubated for 48 h to ensure complete cell attachment to the well. The culture medium was replaced with 100 μL of fresh medium containing different concentrations of the test compounds (**7** (0.9, 1.7, 3, 6.7, 13, 27, 54, 107 μM); **8** (2, 4, 8, 16, 32, 64, 128, 255 μM); **9** (1.3, 2.5, 5.10, 20, 40, 81, 162 μM); **10** (1.3, 2.5, 5.10, 20, 40, 81, 162 μM); DXR (0.08, 0.16, 0.31, 0.63, 1.25, 2.5, 5, 10 μM); 5-FU (8, 16, 31, 63, 125, 250, 500, 1000 μM); and DMSO vehicle (0.008, 0.016, 0.031, 0.063, 0.125.0.25, 0.5, 1%)). Cells were further incubated for 48 h, and the number of viable cells relative to the control was determined via the MTT assay, which is based on MTT metabolism to formazan by viable cells, as described previously [20]. In brief, cells were incubated in the microplate for 2 h with 0.2 mg/mL MTT, the purple formazan precipitate was solubilized by adding 100 μL DMSO, OD560 was recorded on a microplate reader (Infinite F50R; TECAN, Männedorf, Switzerland), and the readings were adjusted for cytotoxicity caused by the vehicle. The concentration of test compound that produced cytotoxicity by 50% (CC_{50}) was determined in triplicate from the dose–response curves.

CC_{50} values against three normal human oral mesenchymal cell lines (HGF, HPLF, and HPC) and four OSCC cell lines (Ca9-22, HSC-2, HSC-3, and HSC-4) were determined. The mean CC_{50} values for the normal and tumor cell lines were calculated and the ratio of the means gives the tumor specificity (TS):

$$TS = \text{mean } CC_{50} \text{ normal cell lines} / \text{mean } CC_{50} \text{ OSCC cell lines}$$

2.5.3. Statistical Analysis

All analyses were carried out in triplicate to ensure robustness and reliability. The data are presented as mean ± standard deviation (SD). Graph Pad Prism 7 and Microsoft Excel 2010 were used for the statistical and graphical evaluations.

3. Results and Discussions

3.1. Structure Determination of the Isolated Compounds

A 70% aq acetone extract of *L. inermis* leaves was fractionated using a Diaion HP-20 gel (2.3. Extraction and Isolation). The multistep isolation using gel chromatography combined with preparative HPLC purification afforded a new megastigmane glucoside gallate (**1**, Figure 2), along with the known benzyl 6′-O-galloyl-β-D-glucopyranoside (**2**) from the

Diaion 75% aq MeOH fraction, and benzoic acid (**3**) and ellagic acid (**4**) from the Diaion MeOH fraction. In addition, two O-glycosidic ellagitannins, heterophylliin A (**5**) and gemin D (**6**), and four C-glycosidic ellagitannins, lythracin D (**7**), pedunculagin (**8**), flosin B (**9**), and lagerstroemin (**10**) were purified from the Diaion 50% aq MeOH eluate.

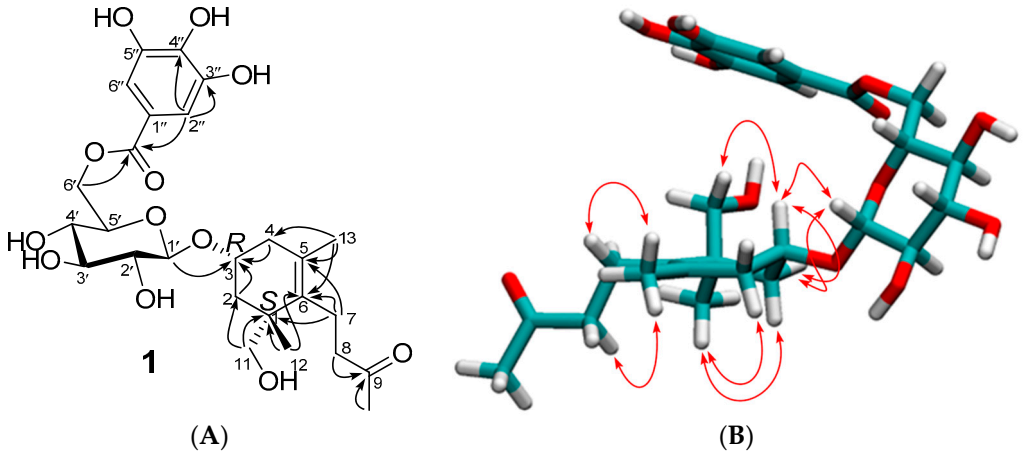

Figure 2. Structure of new megastigmane (**1**). (**A**) Key HMBC correlations. (**B**) Important NOESY correlations.

3.1.1. Structure of the New Megastigmane (**1**)

Compound **1** was isolated as a colorless gummy solid, and its molecular formula, $C_{26}H_{36}O_{12}$, was established from the HRESIMS molecular ion peak at m/z 563.2072 $[M + Na]^+$ (calculated for $C_{26}H_{36}O_{12}Na$, 563.2099) and m/z 539.2128 $[M - H]^-$ (calculated for $C_{26}H_{35}O_{12}$, 539.2134), as well as the ^{13}C NMR data (Table 1). The ^1H NMR spectrum of **1** (Figures S3–S5) displayed spectroscopic features typical of a galloyl moiety [22]; an aromatic 2H singlet (δ_H 7.13, H-2″/H-6″) that exhibits HSQC correlation with a non-oxygenated aromatic carbon (δ_C 109.6, 2C, C-2″/C-6″) and HMBC correlations with oxygenated aromatic carbon (δ_C 146, 2C, C-3″/C-5″, and δ_C 137.7, C-4″), a quaternary aromatic carbon (δ_C 120.5, C-1″), and a carbonyl carbon (δ_C 167.2, C-7″). The ^1H NMR and ^1H–^1H COSY spectra of **1** (Table 1, Figures S6–S8) exhibited a resonating system of seven aliphatic proton spins at δ_H 4.49–3.19 (Table 1), with a large coupling pattern of the glucose H-2′–H-5′ ($J_{H\text{-}1'\text{–}H\text{-}2'}$ = 7.8, $J_{H\text{-}2'\text{–}H\text{-}3'} = J_{H\text{-}3'\text{–}H\text{-}4} = J_{H\text{-}4'\text{–}H\text{-}5'}$ = 9.6 Hz), highlighting the $^4C_1$ conformation of the glucopyranose moiety [23]. A large coupling constant of the glucose H-1′ proton signal (δ_H 4.49, J = 7.8 Hz) indicates the β-configuration of the glucose's anomeric center [22]. The HSQC correlations of the glucose proton signals (Figure S10) enabled the assignments of the ^{13}C chemical shifts (δ_C 102.2, 74.5, 77.5, 71.3, 74.8, 64.8) to the glucose carbons C-1′–C-6′, respectively (Table 1). The ^{13}C NMR spectrum of **1** (Figure S9) also exhibited a system of thirteen carbons (Table 1), characteristic of the megastigmane moiety [24]. Aided by the ^1H–^1H COSY and HSQC spectroscopic data, the system is separated into two components. The first is composed of nine carbons, recognized by their 1D NMR and the HSQC data: one oxygenated methine carbon δ_C 72.3 (C-3) (correlated in the HSQC spectrum to a 1H multiplet signal at δ_H 4.14 (H-3)), two non-oxygenated methylene carbons at δ_C 41.6 (C-2) (correlated in the HSQC spectrum to the H_2-2 proton signals at δ_H 1.21 (1H, t, J = 8.4 Hz, H-2ax) and 2.25 (1H, ddd, J = 2.4, 5.4, 14.4 Hz, H-2eq) and at δ_C 39.2 (C-4) (correlated in the HSQC spectrum to the H_2-4 proton signals at δ_H 1.94 (1H, br.dd, J = 9.6, 16.2 Hz, H-4ax) and δ_H 2.30 (1H, dd, J = 5.4, 16.2 Hz, H-4eq)), one oxygenated methylene carbon at δ_C 68.6 (C-12) (correlated in the HSQC spectrum to δ_H 3.39 and 3.28 (each 1H, d, J = 11 Hz)), two tetrasubstituted olefinic carbons at δ_C 128.8 (C-5) and 136.6 (C-6), and a quaternary carbon at δ_C 43.5 (C-1). The remaining two methyl carbons of this component appear at δ_C 24.3 and 19.8, and one of them is correlated in the HSQC with a 3H-singlet at an up-field shift of 0.91 (H3-11), and the other is correlated with the proton signal at a relatively low-field shift δ_H 1.54 (3H, brs, H_3-11). The ^1H chemical shift

of the latter corresponds to the methyl group on an olefenic carbon, and the broadening of the signal is explained by the W-shaped ^{1}H–^{1}H coupling with the H-4 proton signal (δ_H 1.94, 1H, br.dd) [25]. The second component of the megastigmane moiety was found to be composed of a chain of four carbons: the 1D together with the 2D (^{1}H–^{1}H COSY, Figures S6–S8) and HSQC (Figures S10–S12) spectra substantiated the presence of two methylene groups (δ_H 2.14 and 2.2 (2H, dd, H_2-7), correlated with a carbon signal at δ_C 22.3 (C-7) and δ_H 2.48 (2H, t, H_2-8), correlated with a carbon signal at δ_C 44.2 (C-8)). The other two carbons were identified as methyl and ketone carbons: the methyl proton signal at δ_H 2.08 (3H, s, H_3-10) exhibits an HSQC correlation with the carbon peak at δ_C 29.8 (C-10) and an HMBC correlation with a ketonic carbonyl carbon peak at δ_C 209.3. The same carbonyl carbon is also correlated with the H_2-8 signal at δ_H 2.48 in the HMBC spectrum. This four-carbon segment, proposed as $–CH_2–CH_2–CO–CH_3$, was placed at the olefenic carbon C-6 (δ_C 133.6), as deduced from the HMBC correlations of the H-7 signal at δ_H 2.14 with C-6 (δ_C 133.6) and the neighboring carbons C-1 (δ_C 43.5) and C-5 (δ_C 128.8). The connectivity of the structural components (galloyl, glucosyl, and megastigmane moieties) of **1** was then substantiated based on the HMBC correlations (Figures S13 and S14).

Table 1. The 1D (^{1}H, ^{13}C NMR) and 2D (HMBC and NOESY) spectroscopic data of compound **1**.

Position	δ_H	δ_C	HMBC	NOESY
1		43.5		
2ax	1.21, 1H, t (12.6)	41.6	C-2, C-3, C-4, C-11, C-12	H-11, H-2ex
2eq	2.25, 1H, br.dd (8.4, 14.4)		C-1	H-2aq
3	4.14, 1H, m	72.8		H-1′, H-4eq, H-12
4ax	1.94, 1H, br.dd (9.6, 16.8)	39.2	C-3, C-5, C-6	H-11, H-4eq
4eq	2.30, 1H, br. dd (5.4, 16.8)		C-2, C-5, C-6	H-4ax
5		128.8		
6		133.6		
7	2.14, 1H, dd (8.4, 14.4) [a], 2.20, 1H, dd (8.4, 14.4) [a]	22.3	C-5, C-6, C-8, C-9	H-11, H-13
8	2.48, 2H, t (8.4)	44.2	C-7, C-9	H-11, H-13
9		209.3		
10	2.08, 3H, s	29.8 [b]	C-8, C-9	H-7
11	3.39, 1H, d (11),	68.6	C-1, C-2, C-11	H-3
11	3.28, 1H, d (11)			
12	0.91, 3H, s	24.3	C-1, C-2, C-6, C-12	H-2ax, H-4ax, H-7, H-8
13	1.54, 3H, br.s	19.8	C-4, C-5, C-6	H-7, H-8
1′	4.49, 1H, d (7.8)	102.2	C-3	H-3, H-4eq
2′	3.19, 1H, dd (7.8, 9.6)	74.5	C-1′, C-3′	
3′	3.44,1H, t (9.6)	77.5	C-2′, C-4′	
4′	3.35,1H, t (9.6)	71.3	C-3′, C-5′, C-6′	
5′	3.61, 1H, ddd (1.8, 9.6,	74.8	C-3′, C-4′	
6′	4.61,1H, dd (1.8, 13.8)	64.8	C-5′, C-7″	
	4.16, 1H, dd (7.2, 12.0)			
1″		120.5		
2″/6″	7.13, 2H, s	109.6		
3″/5″		146		
4″		137.7		
7″		167.2		

[a] Approximate multiplicity because proton signal overlapped with solvent impurities; [b] Hidden under the solvent peaks and identified from HSQC correlation with δ_H 2.08 (H_3-10), which together with H_2-8 (δ_H 2.48, 2H, t) exhibited HMBC correlations with C-9 (δ_C 209.3).

The galloyl unit was positioned on the glucose C-6′; this was based on the low-field shift of the glucose C-6′ signal (δ_C 64.8) in addition to a weak HMBC correlation of glucose-H-6 (δ_H 4.16) with the galloyl carbonyl carbon peak (δ_C 167.2). The down-field shift of the glucose anomeric carbon (δ_C 102.2, C-1′) indicated the presence of an *O*-glucosidic linkage

between the megastigmane aglycone and glucose C-1′, which was confirmed by the HMBC correlation of the glucose H-1′ (δ_H 4.49) and the megastigmane moiety C-3 (δ_C 72.8).

The ^{1}H NMR spectrum showed the H-3 signal at δ_H 4.14 as a multiplet in the ^{1}H NMR spectrum, where the coupling constants of $J_{2ax\text{-}3}$, $J_{2eq\text{-}3}$, $J_{4ax\text{-}3}$, and $J_{4eq\text{-}3}$ with the adjacent proton signals were assigned to be 12.6 Hz, 8.4 Hz, 9.6 Hz, and 5.4 Hz, respectively. These NMR data indicated the equatorial orientation of the substituted hydroxyl group at C-3. This was further evidenced by the ^{1}H-^{1}H nuclear Overhauser effect spectroscopy (NOESY) correlations between the axially oriented glucose H-1′ proton (δ_H 4.49) and both H-3 (δ_H 4.14) and H-4eq (δ_H 2.30) (Figures S15–S17) corresponding to the *R* chirality of C-3 in compound **1** [26]. In the skeleton of megastigmanes, it has been documented, thus far, that the hydroxyl group at the C-3 position frequently has an equatorial orientation [27]. The NOESY spectrum exhibited a key correlation of H-3 with H_2-11 and NOESY correlations of both H-2ax (δ_H 1.21, t) and H-4ax (δ_H 1.94) with H_3-12 (δ_H 0.91, 3H, s, methyl), indicating the *S* chirality of C-1. Among the four possible stereoisomers (1*S*3*S*, 1*R*3*R*, 1*S*3*R*, and 1*R*3*S*, Figure S41) of **1**, these NOESY correlations were consistent with the 1*S*3*R* isomer. The H_3-12 methyl signal, as well as the H_3-13 methyl signal (δ_H 1.54, 3H, s), exhibited NOESY correlations with H_2-7 (δ_H 2.14 and 2.20) and H_2-8 (δ_H 2.48). The NOESY correlations between each pair of protons of H_2-2 and H_2-4 and H_2-7 were also detected (Figures S15–S17). Importantly, the practically recoded ECD spectrum of **1** was compared with the computationally calculated ECD (see procedures in the Supplementary Materials) of the four possible stereoisomers. Despite the noisy Cotton effects of the practically measured ECD, the overall spectrum was consistent with that calculated for the 1*S*3*R* isomer (Figure S42). According to these findings, the new structure of **1** was concluded to be a gallate derivative of a megastigmane glucoside, as shown in Figure 2, and given the name lawsoiononoside (**1**).

Except for the megastigmane aglycone *β*-ionone, this is the first report on the isolation of a megastigmane from henna. Megastigmanes are oxygenated isonorterpenoids with a C13 carbon skeleton and frequently referred to as oxidative by-products from *β*-carotenoids [28]. The biosynthesis of compound **1** from *β*-ionone and gallic acid is assumed to be as shown in Figure 3. This biotransformation involves the oxidation of C-3 and C-11 of the megastigmane basic skeleton (Step A), followed by the glucosylation (Step B) and esterification of the glucose OH-6 with gallic acid (Step C). Direct glycosylation of the megastigmane with a 6-*O*-galloyl glucose is also possible.

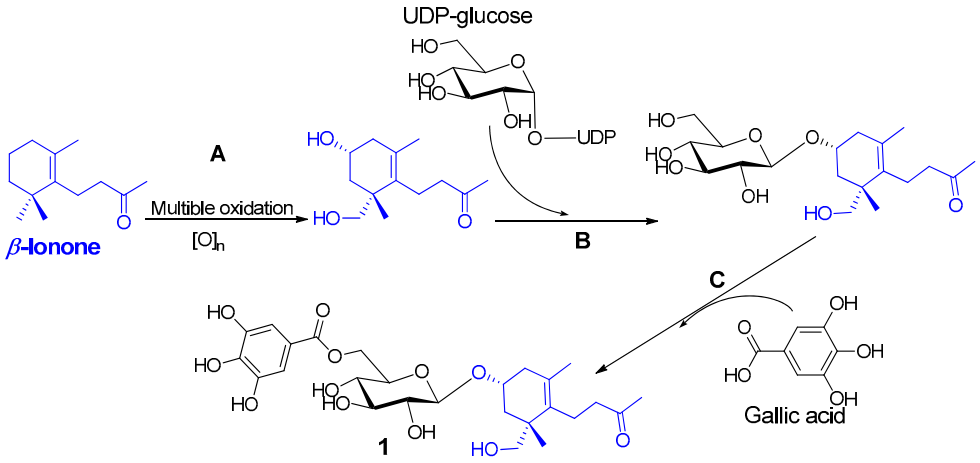

Figure 3. Suggested biosynthesis of compound **1** from β-ionone and gallic acid.

Numerous megastigmane glucosides have been shown to have antibacterial, anti-inflammatory, anticancer, and hepatoprotective effects, which are strongly correlated with their antioxidant capacity [29–31]. The antioxidant activity of megastigmane glycosides has been demonstrated through their capacity to scavenge DPPH free radicals and suppress

the process of lipid peroxidation [31]. The bioactivities of this class of metabolites, coupled with their antioxidant power, suggests the need for further studies in the future on these intriguing bioactive small molecules as a scaffold of drug discovery.

3.1.2. Structure of Known Compounds (**2**–**10**)

Structure of Compounds **2**–**4**

- Benzoic acid (**3**), together with the tannin-related metabolite benzyl 6′-*O*-galloyl-β-D-glucopyranoside (**2**), and ellagic acid (**4**) are isolated for first time from henna, and their structures (Figure 4) were determined from the NMR and ESIMS data referenced to the literature values as follows:

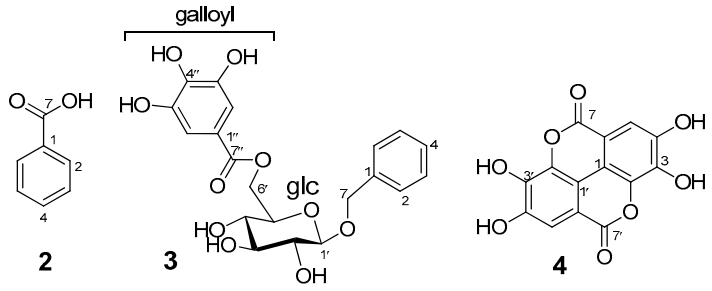

Figure 4. Structures of the compounds **2**–**4**, first isolated from henna.

- Compound **2** was isolated as **a** colorless crystalline solid. Its structure was identified from the ^{1}H NMR pattern of a monosubstituted benzene [δ_H 7.95 (2H, dd, J = 1.8, 7.2 Hz, H-2/H-6), 7.62 (1H, tt, J = 1.8, 7.2 Hz, H-4), and 7.50 (2H, dd, J = 7.2, 7.2 Hz, H-3/H-5)] (Figure S18) and the ^{13}C NMR data δ_C 132.89 (C-4), 130.7 (C-1), 129.2 (C-2/C-6), and 128.5 (C-3/C-5) (Figure S20), which are consistent with a monosubstituted benzene as well. The presence of a carboxyl group was recognized by a broad proton signal in the low-field region (δ_H 12.9) and a carbonyl carbon peak at δ_C 167.23 (C-7). The ESIMS molecular ion peak at m/z 121 $[M–1]^-$ confirmed the identification of **2** as a benzoic acid [15].
- Compound **3** was isolated as a white amorphous powder. Its 1H NMR spectrum (Figure S22) exhibited proton signals of a $^{1}C_4$ β-D-glucopyranose core {δ_H 4.55 [1H, dd, J = 1.8, 12 Hz, glc H-6], 4.39 (1H, d, J = 8.4 Hz, glc H-1), 4.34 (1H, dd, J = 6.6, 12.6 Hz, glc H-6), 3.29 (1H, dd, J = 8, 9 Hz, glc H-2), 3.44 (1H, t, J = 9 Hz, glc H-3), 3.44 (1H, t, J = 9 Hz, glc H-4), and 3.57 (1H, ddd, J = 1.8, 6, 9 Hz, glc H-5)} [12,13,22]. The spectrum also exhibited a 2H singlet at δ_H 7.13 (2H, s, galloyl H-2/H-6), which exhibited a HSQC correlation with the 2C peak at δ_C 109.7 (2C, galloyl C-2/C-6). These are characteristic of a galloyl moiety [12,13,22]. The spectrum also exhibited a proton signal of a benzyl moiety at δ_H 7.33 (2H, dd, J = 1.2, 7.8 Hz, H-2/H-6), 7.26 (2H, dt, J = 1.2, 7.8 Hz, H-3/H-5), 7.20 (1H, dt, J = 1.2, 7.8 Hz, H-4), and 4.79, 4.59 (each 1H, d, J = 12 Hz, H-7). The ^{13}C NMR spectrum (Figure S24) exhibited carbon peaks corresponding to the structural components of **2** (*viz*, benzyl, galloyl, and glucose). The HMBC correlations between the galloyl 2H singlet (δ_H 7.13) and the glucose H_2-6 (δ_H 4.55 and 4.34) with the galloyl carbonyl carbon (δ_C 167.2) evidenced the placement of the galloyl moiety at C-6 of the glucose core. The HMBC correlations of the benzyl H_2-7 at δ_H 4.79 and 4.59 (each 1H, d, J = 12 Hz) with the glucose anomeric carbon (δ_C 102.7), as well as the HMBC correlation of the glucose anomeric proton (δ_H 4.39) with the benzylic carbon C-7 (δ_C 70.9), indicated the placement of the benzyl moiety at the anomeric center of the glucose, as shown by the structural formula of **2** (Figure 4). The ESIMS negative ion peak at m/z 421 $[M - H]^-$ confirmed the identification of **2** as benzyl 6′-*O*-galloyl-*β*-D-glucopyranoside [16]. Compound **4** was isolated as a pale yellow amorphous powder. Its ^{1}H NMR spectrum (Figure S27) exhibited a 2H singlet signal at δ_H 7.50 (H-2/H-2′) and a broad singlet at δ_H 10.69 (br. s, OH). The ^{13}C NMR spectrum exhibited seven carbon peaks, each equivalent to two carbons [δ_C 159.5 (2C,

C-7/C-7′), 148.5 (2C, C-4/C-4′), 140.0 (2C, C-2/C-2′), 136.8 (2C, C-3/C-3′), 112.7 (2C, C-6/C-6′), 110.6 (2C, C-5/C-5′), and 108.0 (2C, C-1/C-1′). These are characteristics for an ellagic acid. Based on the molecular ion peak at m/z 301 $[M - H]^-$ in the ESIMS spectrum, we confirmed the structure of **4** to be ellagic acid [17].

It is worth noting that Ye et al., 2007, have reported two resonances (δ_H 7.14 and 7.47) for the equivalent ellagic acid protons (H-5 and H-5′, respectively), which are incorrect and misleading NMR data [32].

Structure of the *O*-Glycosidic Ellagitannins **5** and **6**

Heterophylliin A (**5**) and gemin D (**6**) were isolated first from the plant, and hence, their structures were determined from the following spectroscopic data and comparison with the literature values:

- Compound **5** was isolated as an off-white amorphous powder. Its ^{1}H NMR spectrum (Figure S29) exhibited aromatic proton signals at δ_H 7.23, 7.03 (each 2H, s, galloyl H-2/H-6) of two galloyl units and two 1H singlets (δ_H 6.61 and 6.48), indicative of the presence of a hexahydroxydiphenoyl (HHDP) unit [22]. A spin system of seven aliphatic proton sets, as evident from the ^{1}H–^{1}H COSY correlations (Figure S30), were assigned for the $^4C_1$ D-glucopyranose core as follows: δ_H 6.39 (1H, d, J = 4.2 Hz, glc H-1), 5.64 (1H, t, J = 10.2 Hz, glc H-3), 5.22 (1H, dd, J = 13.2, 6.6 Hz, glc H-6), 5.05 (1H, t, J = 10.2 Hz, glc H-4), 4.55 (1H, br. dd, J = 6.6, 10.2 Hz, glc H-5), 4.20 (1H, dd, J = 4.2, 10.2 Hz, glc H-2), and Hz, 3.75 (1H, br. d, J = 13.2 Hz, glc H-6). The up-field shift of the glucose H-2 signals (δ_H 4.20) indicated the deacylation of the glucose 2-OH, whereas the small coupling constant (J = 4.2 Hz) of the anomeric proton signal indicated the alpha-oriented C-O bond at the glucose's anomeric center [14,18]. The large difference in the chemical shifts of the glucose H_2-6 signals (δ_H 4.20 and 3.75) indicated the placement of the HHDP group at O-4/O-6 of the glucose, and therefore, the remaining O-1 and O-3 should be acylated by the galloyl units [14]. These data, together with the comparison with the literature values [18], led to the identification of **5** as heterophylliin A (**5**, Figure 5).

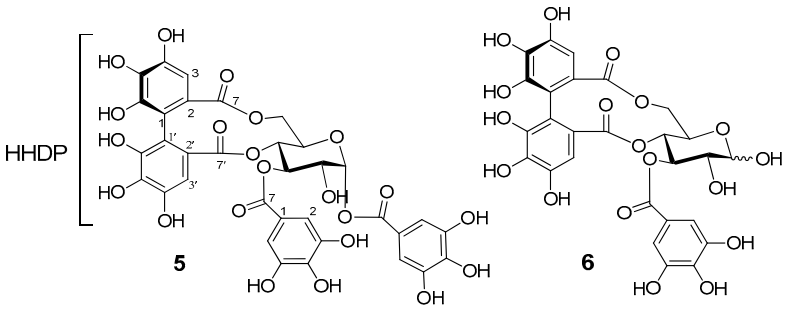

Figure 5. Structure of the ellagitannins **5** and **6**.

- Compound **6** was isolated as an off-white amorphous powder. Its ^{1}H NMR spectrum exhibited double resonances of all proton signals (Section 2.4. Spectroscopic Data of Isolated Compounds), which indicated the existence of **6** as a mixture of α- and β-anomer. The aromatic proton signals [δ_H 7.01, 7.00 (each s, 2H in total), δ_H 6.59, 6.58 (each s, 1H in total), and δ_H 6.44, 6.43 (each s, 1H in total) are consistent with the galloyl H-2/H-6, HHDP H-3, and HHDP H-3′, respectively [22]. Proton signals of a glucose core [δ_H: 5.46, 5.28 (1H in total, each t, J = 10.2 Hz, glc H-3α, β), 5.24 (1/2H, d, J = 4.2 Hz, glc H-1α), 5.21, 5.18 (1H in total, each dd, J = 6.6, 10.2 Hz,), 4.95, 4.92 (1H in total, each t, J = 10.2 Hz, H-4α, β), 4.72 (1/2H, d, J = 7.2 Hz, H-1β), 4.52, 4.06 (1H in total, each ddd, J = 1.2, 6.6, 10.2 Hz, H-5α, β), 3.81 (1/2H, dd, J = 4.2, 10.2 Hz, H-2α), 3.78, 3.71 (1H in total, each dd, J = 1.2, 13.2 Hz, H-6α, β), and 3.57 (1/2H, dd, J = 7.2, 10.2 Hz, H-2β) were detected in the NMR spectrum of **6**. These

double resonances indicate the presence of the unacylated OH group of the anomeric center [14]. Resonances of the glucose H-2 signals with the up-field shifts (δ_H 3.81 and 3.57) also evidenced the existence of the free OH-2 on the glucose core. Similar to heterophylliin A (**5**), the wide difference in the chemical shifts of the glucose H_2-6 signals (δ_H 5.21, 5.18, H-6α, β, and δ_H 3.78, 3.71, H-6α, β) indicated the bridging of the HHDP moiety at O-4/O-6 of the glucose core, leaving the glucose O-3 for the galloyl moiety. These spectroscopic data, which are reasonably identical with those previously published, confirmed the identity of **6** as gemin D (Figure 5) [19].

Structure of *C*-Glycosidic Ellagitannins (**7**–**10**)

The *C*-glycosidic ellagitannins **7**–**10** (Figure 6) are known compounds which were previously isolated from the same plant resource. Their structures were identified from NMR data (Section 2.4. Spectroscopic Data of Isolated Compounds and Figures S33–S40) and compared with the published NMR data as lythracin D (**7**), pedunculagin (**8**), flosin B (**9**), and lagerstroemin (**10**) [13].

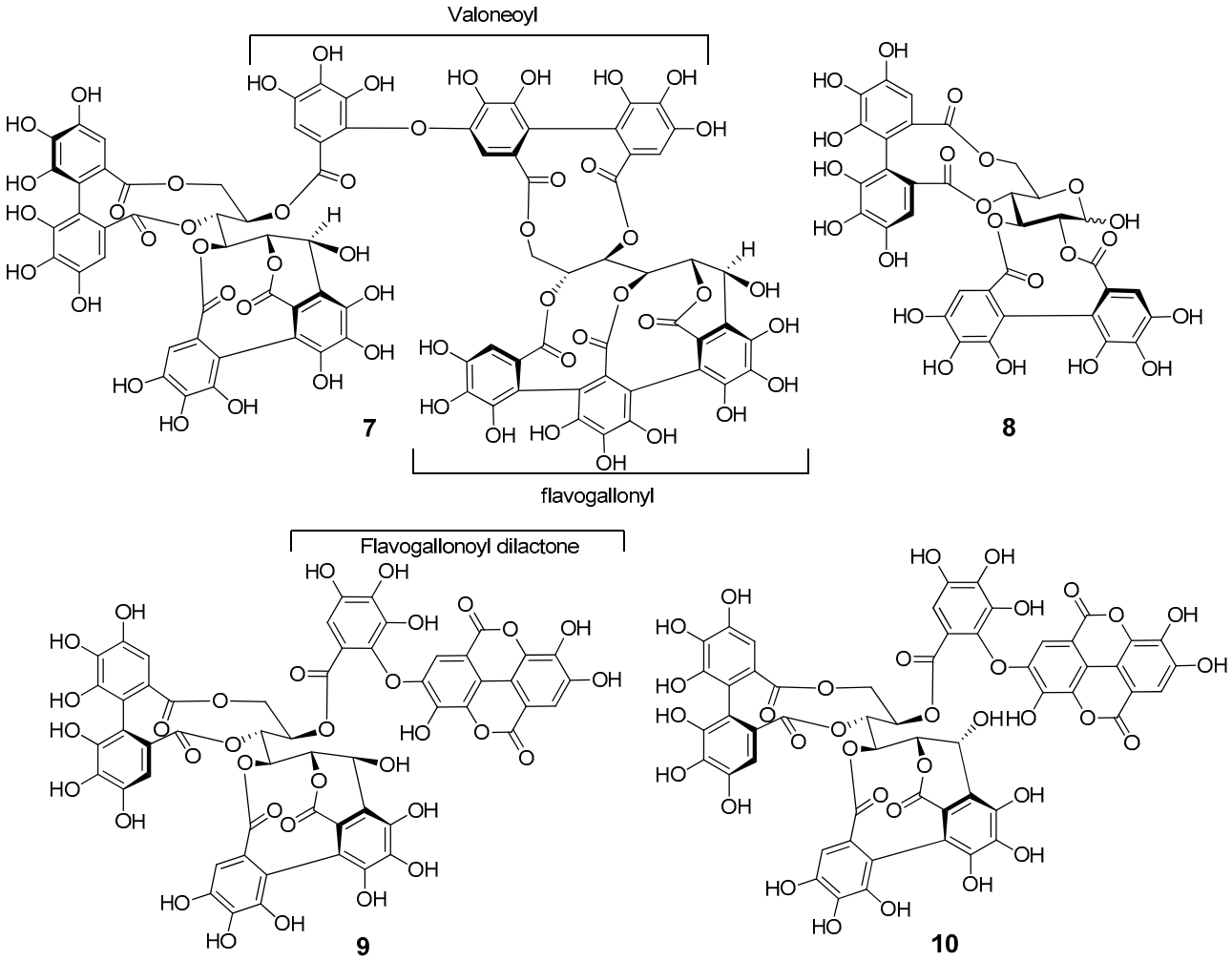

Figure 6. Structures of the known ellagitannins **7**–**10**.

3.2. Cytotoxicity of Ellagitannins against Oral Cancer Cell Lines

The anticancer properties of *L. inermis* leaf, root, flower, and bark extracts have been thoroughly studied using animal models and cancer cell lines [33]. Water extracts of *L. inermis* leaves inhibited the growth of various cancer cell lines to varying degrees [34,35].

In the current study, four *C*-type glycosidic ellagitannins, which are typical of lythraceae plants, were among the isolated groups of phytochemicals that were detected in high con-

centrations in the aqueous acetone extract of henna leaves. Lately, it has become more common to investigate the applicability of ellagitannins to treat illnesses brought on by oxidative stress, such as cancer and neurodegenerative diseases [36]. Ellagitannins from various plants have demonstrated prominent multi-mechanistic antitumor properties [37]. The selective cytotoxicity against human oral squamous cell carcinoma (OSCC) vs. normal oral cells was examined for four ellagitannins: lythracin D (**7**), flosin B (**9**), lagerstroemin (**10**), of unknown cytotoxicity, and pedunculagin (**8**), a known antitumor agent [38–40]. All four ellagitannins, as well as doxorubicin (DXR), were cytotoxic toward the OSCC cell lines, whereas 5-FU was cytostatic. Pedunculagin and lythracin D demonstrated significant tumor-specific cytotoxicity (TS = 2.8 and 2.3, respectively), while flosin B and lagerstroemin exhibited low specificity (TS = 1.7 and 1.5, respectively) (Table 2). The primary mechanism by which ellagitannins and their derivatives, including ellagic acid, exhibit anticancer activities is through their antioxidant capacity, which is dependent on both iron chelation activity and direct radical scavenging and varies with the degree of hydroxylation [41]. According to the literature, ellagitannins' antitumor properties are primarily influenced by their antioxidant activity and their ability to reduce inflammation; research-based evidence suggested that they have the ability to regulate secretory growth factors and proinflammatory molecules like IL-6, TGF-β, TNF-α, IL-1β, and IFN-γ [42]. Research has demonstrated that a number of oligomeric ellagitannins have in vivo anticancer effects against mouse models of sarcoma 180 and MM2, which was linked to a strengthened host immune response. In vitro research using tumor cell lines has shown that a number of ellagitannins, as well as their constituent acids gallic and ellagic, showed a strong cytotoxicity against carcinoma cell lines and a low cytotoxicity toward normal cells [20]. Our findings in the present study are consistent with the previous reports on ellagitannin's cytotoxic activity [20,42] and highlight the potential of the development of *L. inermis* ellagitannins as anti-oral cancer drugs. Furthermore, the occurrence of *C*-type glycosidic ellagitannins in abundance is significant from a chemotaxonomic perspective as well as for explaining the multiple biological benefits of henna, such as its anti-inflammatory, antioxidant, and anticancer properties.

Table 2. Cytotoxicity of ellagitannins **7**–**10** against human OSCC cell lines and normal oral cells [a].

	CC_{50} (μM) [b]				CC_{50} (μM) [b]				
	Ca9-22	**HSC-2**	**HSC-4**	**Mean**	**HGF**	**HPLF**	**HPC**	**Mean**	**TS [c]**
Lythracin D (7)	89 ± 4	67 ± 8	48 ± 10	68	157 ± 36	152 ± 5	152 ± 4	154	2.3
Pedunculagin (8)	93 ± 5	48 ± 4	48 ± 3	63	178 ± 11	187 ± 4	157 ± 7	174	2.8
Flosin B (9)	180 ± 18	66 ± 8	80 ± 4	109	200	174 ± 22	169 ± 14	181	1.7
Lagerstroemin (10)	185 ± 14	75 ± 11	87 ± 2	115	200	159 ± 9	155 ± 5	171	1.5
Doxorubicin	0.5 ± 0.05	0.16 ± 0.04	0.17 ± 0.01	0.29	10 ± 0	10 ± 0	10 ± 0	10	>35
5-FU	33 ± 12	10 ± 2	35 ± 6	26	1000 ± 0	1000 ± 0	1000 ± 0	1000	>38.0

[a] Ca9-22, HSC-2, and HSC-4 are oral squamous cell carcinoma (OSCC) cell lines. HGF, HPLF, and HPC are the normal oral cells. [b] Results are expressed as the mean ± SD of three independent experiments. [c] TS = [CC_{50} (HGF) + CC_{50} (HPLF) + CC_{50} (HPC)]/[CC_{50} (Ca9-22) + CC_{50} (HSC-2) + CC_{50} (HSC-4)].

*3.3. Previously Reported Bioactivities of the Known Compounds **2**–**10***

L. inermis is a medicinal plant that is popular in Unani medicine and ancient Egyptian medical papyri, with promising biological attributes: strong fungicidal, antibacterial, virucidal, antiparasitic, antiamoebiasis, astringent, and antihemorrhagic [4,5]. In addition, henna's plant extracts were found to be effective sedative, hypotensive, anti-Alzheimer's, antioxidant, hepatoprotective, immunomodulatory, and anticancer agents [3,6–8,10,43]. In this study, we report on the isolation and structural identification of a megastigmane (**1**) as well as several ellagitannins and tannin-related phenolics. Reviewing biological studies conducted on these compounds (Table 3) emphasized the above-mentioned biological qualities of henna.

Table 3. Reported pharmacological activities of isolated compounds **2**–**10**.

Compound	Reported Biological Activity
benzyl-6′-*O*-galloyl-β-D-glucopyranoside (2)	Antifungal activity against *C. albicans* clinical isolates and reference strains [44]. Moderate inhibitory effects against lipopolysaccharide-induced nitric oxide production in RAW 264.7 cells [45].
Benzoic acid (3)	Antibacterial and antifungal activity [46].
Ellagic acid (4)	Antioxidant, anti-inflammatory, antimutagenic, antiproliferative, antiallergic, antiatherosclerotic, cardioprotective, hepatoprotective, nephroprotective, and neuroprotective properties [47].
Heterophylliin A (5)	Antidiabetic (moderate inhibitory effect against dipeptidyl peptidase IV and α-glucosidase) activity [48]. Antioxidant, antiallergic, and anti-inflammatory [49].
Gemin D (6)	Cytotoxic and chemo-preventive, in vitro anti-HIV activity, anti-Leishmania donovani amastigote, a potent growth-inhibitor of sarcoma 180 cells in mice. A potent inhibitory effect as a 3-hydroxy-3-methylglutaryl-coenzyme-A reductase [50]. In vivo antigenotoxic activity [51].
Lythracin D (7)	Anticholinesterase [13], cytotoxic to OSCC cell lines [12].
Pedunculagin (8)	Anti-acne vulgaris (mediated by anti-inflammatory activity and 5α-reductase inhibition) [52], antibacterial, and antihemolytic [53]. Antitumor activity [38–40].
Flosin B (9)	Contributes to the antidiabetic activity of *Lagerstroemia speciosa* by increasing glucose uptake of rat adipocytes [54]. Anti-acetylcholinesterase [13].
Lagerstroemin (10)	Increased glucose uptake of rat adipocytes and could be responsible for lowering of blood glucose level, as shown by *Lagerstroemia speciosa* extract [54].

4. Conclusions

To further our search for the exploration of new phytomolecules from polyphenolic-rich plants, we isolated ten compounds with various characteristics from *L. inermis* leaves. The novel megastigmane structure lawsoiononoside (**1**) is also reported here based on intensive spectroscopic data. Given the interesting bioactivities of megastigmanes [29–31], our discovery of **1** will spur an additional exploration of the unique megastigmane structures from *L. inermis*. The cytotoxicity of the ellagitannins lythracin D (**7**) and pedunculagin (**8**) against the OSCC cell lines indicates the potential development of anti-oral cancer therapeutics based on *L. inermis*. According to recent studies, ellagitannins' antioxidant, and anti-inflammatory properties, which include the ability to modulate proinflammatory mediators including IL-6, TGF-β, TNF-α, IL-1, and IFN-γ, are mostly involved in their anticancer effects [42]. The tannins **7**–**10**, albeit having a relatively moderate TS, may be an appropriate radiosensitizer to diminish tumor resistance in cancer radiotherapy, as recently shown to be the case for pentagalloyl glucose and a gallotannin-rich extract from *Bouea macrophylla* seed [55]. The different identified chemicals discussed here also draw attention to the numerous biological benefits of henna and encourage additional clinical research in order to benefit from the antibacterial, anti-inflammatory, antioxidant, hepatoprotective, and anticancer properties of this promising ancient plant.

Supplementary Materials: The following supporting information can be downloaded at: https://www.mdpi.com/article/10.3390/antiox12111951/s1, Figure S1: Positive-mode HRESIMS spectrum of compound **1**; Figure S2: Negative-mode HRESIMS spectrum of compound **1**; Figure S3: ^{1}H NMR spectrum of compound **1** [600 MHz, acetone-d_6 + D_2O (9+1)]; Figure S4: Expanded ^{1}H NMR spectrum of compound **1** [600 MHz, acetone-d_6 + D_2O (9+1)]; Figure S5: Expanded ^{1}H NMR spectrum of compound **1** [600 MHz, acetone-d_6 + D_2O (9+1)]; Figure S6: ^{1}H-^{1}H COSY spectrum of compound **1** [600 MHz, acetone-d_6 + D_2O (9+1)]; Figure S7: Expanded ^{1}H-^{1}H COSY spectrum of compound **1** [600 MHz, acetone-d_6 + D_2O (9+1)]; Figure S8: Expanded ^{1}H-^{1}H COSY spectrum of compound **1** [600 MHz, acetone-d_6 + D_2O (9+1)]; Figure S9: ^{13}C NMR spectrum of compound **1** [151 MHz, acetone-d_6 + D_2O (9+1)]; Figure S10: HSQC spectrum of compound **1** [600 MHz, acetone-d6 + D2O (9+1)]; Figure S11: Expanded HSQC spectrum of compound **1** [600 MHz, acetone-d_6 + D_2O (9+1)]; Figure S12: Expanded HSQC spectrum of compound **1** [600 MHz, acetone-d_6 + D_2O (9+1)]; Figure S13: HMBC spectrum of compound **1** [600 MHz, acetone-d_6 + D_2O (9+1)]; Figure S14: Ex-

panded HMBC spectrum of compound **1** [600 MHz, acetone-d_6 + D_2O (9+1)]; Figure S15: NOESY spectrum of compound **1** [600 MHz, acetone-d_6 + D_2O (9+1)]; Figure S16: Expanded NOESY spectrum of compound **1** [600 MHz, acetone-d_6 + D_2O (9+1)]; Figure S17: Expanded NOESY spectrum of compound **1** [600 MHz, acetone-d_6 + D_2O (9+1)]; Figure S18: ^1H NMR spectrum of compound **2** (600 MHz, DMSO-d_6); Figure S19: ^1H-^1H COSY spectrum of compound **2** (600 MHz, DMSO-d_6); Figure S20: ^{13}C NMR spectrum of compound **2** (151 MHz, DMSO-d_6); Figure S21: HSQC spectrum of compound **2** (600 MHz, DMSO-d_6); Figure S22: ^1H NMR spectrum of compound **3** [600 MHz, acetone-d_6 + D_2O (9+1)]; Figure S23: ^1H-^1H COSY spectrum of compound **3** [600 MHz, acetone-d_6 + D_2O (9+1)]; Figure S24: ^{13}C spectrum of compound **3** [151 MHz, acetone-d_6 + D_2O (9+1)]; Figure S25: HSQC spectrum of compound **3** [600 MHz, acetone-d_6 + D_2O (9+1)]; Figure S26: HMBC spectrum of compound **3** [600 MHz, acetone-d_6 + D_2O (9+1)]; Figure S27: ^1H NMR spectrum of compound **4** (600 MHz, DMSO-d_6); Figure S28: ^{13}C NMR spectrum of compound **4** (151 MHz, DMSO-d_6); Figure S29: ^1H NMR spectrum of compound **5** [600 MHz, acetone-d_6 + D_2O (9+1)]; Figure S30: ^1H-^1H COSY spectrum of compound **5** [600 MHz, acetone-d_6 + D_2O (9+1)]; Figure S31: ^1H NMR spectrum of compound **6** [600 MHz, acetone-d_6 + D_2O (9+1)]; Figure S32: ^1H-^1H COSY spectrum of compound **6** [600 MHz, acetone-d_6 + D_2O (9+1)]; Figure S33: ^1H NMR spectrum of compound **7** [600 MHz, acetone-d_6 + D_2O (9+1)]; Figure S34: ^1H-^1H COSY spectrum of compound **7** [600 MHz, acetone-d_6 + D_2O (9+1)]; Figure S35: ^1H NMR spectrum of compound **8** [600 MHz, acetone-d_6 + D_2O (9+1)]; Figure S36: ^1H-^1H COSY spectrum of compound **8** [600 MHz, acetone-d_6 + D_2O (9+1)]; Figure S37: ^1H NMR spectrum of compound **9** [600 MHz, acetone-d_6 + D_2O (9+1)]; Figure S38: ^1H-^1H COSY spectrum of compound **9** [600 MHz, acetone-d_6 + D_2O (9+1)]; Figure S39: ^1H NMR spectrum of compound **10** [600 MHz, acetone-d_6 + D_2O (9+1)]; Figure S40: ^1H-^1H COSY spectrum of compound **10** [600 MHz, acetone-d_6 + D_2O (9+1)]; Experimental procedures of TD-DFT calculation of the ECD spectrum of **1**; Figure S41: Three-dimensional structures of possible stereoisomers of compound **1**; Figure S42: Calculated (**A**) and practically measured (**B**) ECD spectra of compound **1** [56–59].

Author Contributions: Conceptualization, M.A.A.O. and T.H.; methodology, H.S. and T.H.; software, E.A.O.; validation, M.A.A.O., H.S. and T.H.; formal analysis, M.A.A.O., H.S. and E.A.O.; investigation, M.A.A.O. and H.S.; resources, A.A.A.A. and M.M.A.; data curation, M.A.A.O. and E.A.O.; writing—original draft preparation, M.A.A.O., E.A.O., A.A.A.A., M.M.A., H.S., B.A.A.-W. and T.H.; writing—review and editing, M.A.A.O., H.S. and T.H.; visualization, T.H.; supervision, T.H.; project administration, M.A.A.O. and B.A.A.-W.; funding acquisition, B.A.A.-W. and M.A.A.O. All authors have read and agreed to the published version of the manuscript.

Funding: The authors are thankful to the Deanship of Scientific Research at Najran University for funding this work under the Distinguished Research Program (grant code NU/DRP/MRC/12/3).

Institutional Review Board Statement: Not applicable.

Informed Consent Statement: Not applicable.

Data Availability Statement: C:\Users\ASUS\Downloads\NMRSpectroscopic data of the reported compounds are included in the Supplementary Material File and available from the corresponding author upon request.

Acknowledgments: The authors are thankful to the Deanship of Scientific Research at Najran University for funding this work under the Distinguished Research Program (grant code NU/DRP/MRC/12/3).

Conflicts of Interest: The authors declare no conflict of interest.

References

1. Haslam, E. Natural polyphenols (vegetable tannins) as drugs: Possible modes of action. *J. Nat. Prod.* **1996**, *59*, 205–215. [CrossRef]
2. Šamec, D.; Karalija, E.; Šola, I.; Vujčić Bok, V.; Salopek-Sondi, B. The Role of Polyphenols in Abiotic Stress Response: The Influence of Molecular Structure. *Plants* **2021**, *10*, 118. [CrossRef]
3. Zumrutdal, E.; Ozaslan, M.A. Miracle Plant for the Herbal Pharmacy; Henna (*Lawsonia Inermis*). *Int. J. Pharmacol.* **2012**, *8*, 483–489. [CrossRef]
4. Skowrońska, W.; Bazylko, A. The Potential of Medicinal Plants and Natural Products in the Treatment of Burns and Sunburn—A Review. *Pharmaceutics* **2023**, *15*, 633. [CrossRef]
5. Singh, D.K.; Luqman, S. *Lawsonia Inermis* (L.): A Perspective on Anticancer Potential of Mehndi/Henna. *Biomed. Res. Ther.* **2014**, *1*, 112–120. [CrossRef]

6. Hasan, K.M.; Yesmin, S.; Akhter, S.F.; Paul, S.; Sarker, S.; Islam, A.; Wahed, M.I.I.; Khan, M.R.I. Hepatoprotective potentiality of various fractions of ethanolic extracts of *Lawsonia inermis* (henna) leaves against chemical-induced hepatitis in rats. *Biochem. Mol. Biol.* **2016**, *1*, 17–22.
7. Alia, B.H.; Bashir, A.K.; Tanira, M.O.M. Anti-inflammatory, antipyretic, and analgesic effects of *Lawsonia inermis* L.(henna) in rats. *Pharmacology* **1995**, *51*, 356–363. [CrossRef]
8. Mikhaeil, B.R.; Badria, F.A.; Maatooq, G.T.; Amer, M.M.A. Antioxidant and Immunomodulatory Constituents of Henna Leaves. *Z. Für Naturforschung C* **2004**, *59*, 468–476. [CrossRef]
9. Bekir, J.; Mars, M.; Souchard, J.P.; Bouajila, J. Assessment of Antioxidant, Anti-Inflammatory, Anti-Cholinesterase and Cytotoxic Activities of Pomegranate (Punica Granatum) Leaves. *Food Chem. Toxicol.* **2013**, *55*, 470–475. [CrossRef]
10. Barani, M.; Mirzaei, M.; Torkzadeh-Mahani, M.; Nematollahi, M.H. Lawsone-Loaded Niosome and Its Antitumor Activity in MCF-7 Breast Cancer Cell Line: A Nano-Herbal Treatment for Cancer. *DARU. J. Pharm. Sci.* **2018**, *26*, 11–17. [CrossRef]
11. Raja, W.; Pandey, S. Antitumoral effect of *Lawsonia inermis* extract on melanoma tumor-bearing C57BL/6 mice. *Pharmacogn. Mag.* **2020**, *16*, 435. [CrossRef]
12. Orabi, M.A.A.; Sakagami, H.; Umemura, N.; Alyami, H.S.; Hatano, T. Two new *C*-glycosidic ellagitannins and accompanying tannins from *Lawsonia inermis* leaves and their cytotoxic effects. *Fitoterapia* **2021**, *153*, 104925. [CrossRef] [PubMed]
13. Orabi, M.A.A.; Orabi, E.A.; Abdel-Sattar, E.S.; English, A.M.; Hatano, T.; Elimam, H. Structural determination and anti-cholinesterase assay of *C*-glycosidic ellagitannins from *Lawsonia inermis* leaves: A study supported by DFT calculations and molecular docking. *Fitoterapia* **2023**, *164*, 105360. [CrossRef] [PubMed]
14. Okuda, T.; Yoshida, T.; Hatano, T. New Methods of Analyzing Tannins. *J. Nat. Prod.* **1989**, *52*, 1–31. [CrossRef]
15. Trzeciak, K.; Kaźmierski, K.; Drużbicki, K.; Potrzebowski, M.J. Mapping of Guest Localization in Mesoporous Silica Particles by Solid-State NMR and Ab Initio Modeling: New insights into benzoic acid and p-fluorobenzoic acid embedded in MCM-41 via ball milling. *J. Phys. Chem. C* **2021**, *125*, 125–10096. [CrossRef]
16. Isaza, J.H.; Ito, H.; Yoshida, T. A flavonol glycoside-lignan ester and accompanying acylated glucosides from *Monochaetum multiflorum*. *Phytochemistry* **2001**, *58*, 321–327. [CrossRef]
17. Hillis, W.; Yazaki, Y. Properties of some methyl ellagic acids and their glycosides. *Phytochemistry* **1973**, *12*, 2963–2968. [CrossRef]
18. Yoshida, T.; Jin, Z.X.; Okuda, T. Heterophylliins A, B, C, D and E, Ellagitannin Monomers and Dimers from *Corylus heterophylla* FISCH. *Chem. Pharm. Bull.* **1991**, *39*, 49–54. [CrossRef]
19. Lee, M.W.; Tanaka, T.; Nonaka, G.I.; Nishioka, I. Dimeric ellagitannins from *Alnus japonica*. *Phytochemistry* **1992**, *31*, 2835–2839. [CrossRef]
20. Sakagami, H.; Okudaira, N.; Masuda, Y.; Amano, O.; Yokose, S.; Kanda, Y.; Suguro, M.; Natori, T.; Oizumi, H.; Oizumi, T. Induction of apoptosis in human oral keratinocyte by doxorubicin. *Anticancer. Res.* **2017**, *37*, 1023–1029. Available online: https://ar.iiarjournals.org/content/anticanres/37/3/1023.full.pdf (accessed on 1 May 2023).
21. Sakagami, H.; Jiang, Y.; Kusama, K.; Atsumi, T.; Ueha, T.; Toguchi, M.; Iwakura, I.; Satoh, K.; Ito, H.; Hatano, T.; et al. Cytotoxic activity of hydrolyzable tannins against human oral tumor cell lines—A possible mechanism. *Phytomedicine* **2000**, *7*, 39–47. [CrossRef] [PubMed]
22. Orabi, M.A.A.; Taniguchi, S.; Sakagami, H.; Yoshimura, M.; Amakura, Y.; Hatano, T. Hydrolyzable Tannins of Tamaricaceous Plants. 7.1 Structures and Cytotoxic Properties of Oligomeric Ellagitannins from Leaves of *Tamarix Nilotica* and Cultured Tissues Of *Tamarix tetrandra*. *J. Nat. Prod.* **2016**, *79*, 984–995. [CrossRef] [PubMed]
23. Orabi, M.A.A.; Orabi, E.A.; Taniguchi, S.; Sakagami, H.; Yoshimura, M.; Amakura, Y.; Hatano, T. Structures, NMR Spectroscopic Features, and Cytotoxic Properties of Oligomeric Hellinoyl (*m*-GO-*m*-GOG)-Type Ellagitannins from the Galls of *Tamarix Aphylla*. *J. Nat. Prod.* **2019**, *82*, 2682–2695. [CrossRef] [PubMed]
24. Jo, M.S.; Lee, S.; Yu, J.S.; Baek, S.C.; Cho, Y.C.; Kim, K.H. Megastigmane Derivatives from the Cladodes of *Opuntia Humifusa* and Their Nitric Oxide Inhibitory Activities in Macrophages. *J. Nat. Prod.* **2020**, *83*, 684–692. [CrossRef] [PubMed]
25. Ferguson, J.T.; Jiang, Q.; Marro, E.A.; Siegler, M.A.; Klausen, R.S. Long-range coupling in cyclic silanes. *Dalton Trans.* **2020**, *49*, 14951–14961. [CrossRef]
26. Otsuka, H.; Zhong, X.N.; Hirata, E.; Shinzato, T.; Takeda, Y. Myrsinionosides AE: Megastigmane glycosides from the leaves of *Myrsine seguinii* Lev. *Chem. Pharm. Bull.* **2001**, *49*, 1093–1097. [CrossRef]
27. Yu, Q.; Matsunami, K.; Otsuka, H.; Takeda, Y. Staphylionosides A—K: Megastigmane Glucosides from the Leaves of *Staphylea bumalda* DC. *Chem. Pharm. Bull.* **2005**, *53*, 800–807. [CrossRef]
28. Baumes, R.; Wirth, J.; Bureau, S.; Gunata, Y.; Razungles, A. Biogeneration of C13-norisoprenoid compounds: Experiments supportive for an apo-carotenoid pathway in grapevines. *Anal. Chim. Acta* **2002**, *458*, 3–14. [CrossRef]
29. Rao, A.S. Isolation, Absolute Configuration and Bioactivities of Megastigmanes or C13 Isonorterpinoides. *Chem. Int.* **2017**, *3*, 69–91. Available online: https://www.bosaljournals.com/chemint/article/view/57/57 (accessed on 20 January 2023).
30. Ninomiya, K.; Morikawa, T.; Zhang, Y.; Nakamura, S.; Matsuda, H.; Muraoka, O.; Yoshikawa, M. Bioactive Constituents from Chinese Natural Medicines. XXIII. Absolute Structures of New Megastigmane Glycosides, Sedumosides A4, A5, A6, H, and I, and hepatoprotective megastigmanes from *Sedum sarmentosum*. *Chem. Pharm. Bull.* **2007**, *3*, 1185–1191. [CrossRef]
31. Bao, X.-H.; Wang, Q.h.; Bao, B.y.q.e.; Han, J.j.; Ao, W.L.J. Antibacterial and Antioxidant Activities of Megastigmane Glycosides from *Hosta Plantaginea*. *Chem. Nat. Compd.* **2017**, *53*, 614–617. [CrossRef]

32. Ye, G.; Peng, H.; Fan, M.; Huang, C.G. Ellagic Acid Derivatives from the Stem Bark of *Dipentodon Sinicus*. *Chem. Nat. Compd.* **2007**, *43*, 125–127. [CrossRef]
33. Al-Snafi, A.E. A review on *Lawsonia inermis*: A potential medicinal plant. *Int. J. Curr. Pharm. Res.* **2019**, *11*, 1–13. [CrossRef]
34. Ishteyaque, S.; Mishra, A.; Mohapatra, S.; Singh, A.; Bhatta, R.S.; Tadigoppula, N.; Mugale, M.N. In Vitro: Cytotoxicity, Apoptosis and Ameliorative Potential of *Lawsonia Inermis* Extract in Human Lung, Colon and Liver Cancer Cell Line. *Cancer Investig.* **2020**, *38*, 476–485. [CrossRef]
35. Kumar, M.; Chandel, M.; Kaur, P.; Pandit, K.; Kaur, V.; Kaur, S.; Kaur, S. Chemical composition and inhibitory effects of water extract of Henna leaves on reactive oxygen species, DNA scission and proliferation of cancer cells. *EXCLI J.* **2016**, *15*, 842. [CrossRef]
36. Hussain, G.; Huang, J.; Rasul, A.; Anwar, H.; Imran, A.; Maqbool, J.; Razzaq, A.; Aziz, N.; Makhdoom, E.U.H.; Konuk, M.; et al. Putative roles of plant-derived tannins in neurodegenerative and neuropsychiatry disorders: An updated review. *Molecules* **2019**, *24*, 2213. [CrossRef]
37. Senobari, Z.; Karimi, G.; Jamialahmadi, K. Ellagitannins, Promising Pharmacological Agents for the Treatment of Cancer Stem Cells. *Phytother. Res.* **2022**, *36*, 231–242. [CrossRef]
38. Chang, J.H.; Cho, J.H.; Kim, H.H.; Lee, K.P.; Lee, M.W.; Han, S.S.; Lee, D.I. Antitumor Activity of Pedunculagin, One of the Ellagitannin. *Arch. Pharmacal Res.* **1995**, *18*, 396–401. [CrossRef]
39. Kashiwada, Y.; Nonaka, G.I.; Nishioka, I.; Chang, J.J.; Lee, K.H. Antitumor Agents, 129. Tannins and Related Compounds as Selective Cytotoxic Agents. *J. Nat. Prod.* **1992**, *55*, 1033–1043. [CrossRef]
40. Marzouk, M.S.A.; Moharram, F.A.; Mohamed, M.A.; Gamal-Eldeen, A.M.; Aboutabl, E.A. Anticancer and Antioxidant Tannins from Pimenta Dioica Leaves. *Z. Für Naturforschung C* **2007**, *62*, 526–536. [CrossRef]
41. Ismail, T.; Calcabrini, C.; Diaz, A.R.; Fimognari, C.; Turrini, E.; Catanzaro, E.; Akhtar, S.; Sestili, P. Ellagitannins in Cancer Chemoprevention and Therapy. *Toxins* **2016**, *8*, 151. [CrossRef] [PubMed]
42. Iijima, Y.; Bandow, K.; Sano, M.; Hino, S.; Kaneko, T.; Horie, N.; Sakagami, H. In vitro assessment of antitumor potential and combination effect of classical and molecular-targeted anticancer drugs. *Anticancer. Res.* **2019**, *39*, 6673–6684. [CrossRef] [PubMed]
43. Chaibi, R.; Romdhane, M.; Ferchichi, A.; Bouajila, J. Assessment of Antioxidant, Anti-Inflammatory, Anti-Cholinesterase and Cytotoxic Activities of Henna (*Lawsonia Inermis*) Flowers. *J. Nat. Prod.* **2015**, *8*, 85–92. Available online: https://www.cabdirect.org/globalhealth/abstract/20163041893 (accessed on 1 May 2023).
44. De Leo, M.; Braca, A.; De Tommasi, N.; Norscia, I.; Morelli, I.; Battinelli, L.; Mazzanti, G. Phenolic Compounds from Baseonema Acuminatum Leaves: Isolation and Antimicrobial Activity. *Planta Medica* **2004**, *70*, 841–846. [CrossRef] [PubMed]
45. Choi, J.; Cho, J.Y.; Choi, S.J.; Jeon, H.; Kim, Y.D.; Htwe, K.M.; Chin, Y.W.; Lee, W.S.; Kim, J.; Yoon, K.D. Two New Phenolic Glucosides from Lagerstroemia Speciosa. *Molecules* **2015**, *20*, 4483–4491. [CrossRef] [PubMed]
46. Nair, B. Final report on the safety assessment of Benzyl Alcohol, Benzoic Acid, and Sodium Benzoate. *Int. J. Toxicol.* **2001**, *20*, 23–50. [CrossRef] [PubMed]
47. Sharifi-Rad, J.; Quispe, C.; Castillo, C.M.S.; Caroca, R.; Lazo-Vélez, M.A.; Antonyak, H.; Polishchuk, A.; Lysiuk, R.; Oliinyk, P.; De Masi, L.; et al. Ellagic acid: A review on its natural sources, chemical stability, and therapeutic potential. *Oxidative Med. Cell. Longev.* **2022**, *2022*, 3848084. [CrossRef] [PubMed]
48. Yu, Y.H.; Jia, L.; Zeng, H.T.; Yuan, T. Hydrolyzable tannins from flowers of Punica granatum and their anti-diabetic activities. *Zhongguo Zhong Yao Za Zhi* **2022**, *47*, 3258–3264. [CrossRef] [PubMed]
49. Sugimoto, K.; Nakagawa, K.; Hayashi, S.; Amakura, Y.; Yoshimura, M.; Yoshida, T.; Yamaji, R.; Nakano, Y.; Inui, H. Hydrolyzable Tannins as Antioxidants in the Leaf Extract of Eucalyptus Globulus Possessing Tyrosinase and Hyaluronidase Inhibitory Activities. *Food Sci. Technol. Res.* **2009**, *15*, 331–336. [CrossRef]
50. Costa Carneiro, C.; Vieira de Moraes-Filho, A.; Silva Fernandes, A.; da Costa Santos, S.; de Melo e Silva, D.; Chen Chen, L. Cytotoxic and Chemopreventive Effects of Gemin D Against Different Mutagens Using In Vitro and In Vivo Assays. *Anti-Cancer Agents Med. Chem.* **2017**, *17*, 712–718. [CrossRef]
51. Silva Fernandes, A.; Hollanda Véras, J.; Silva, L.S.; Puga, S.C.; Luiz Cardoso Bailão, E.F.; de Oliveira, M.G.; Cardoso, C.G.; Carneiro, C.C.; Da Costa Santos, S.; Chen-Chen, L. Pedunculagin Isolated from *Plinia Cauliflora* Seeds Exhibits Genotoxic, Antigenotoxic and Cytotoxic Effects in Bacteria and Human Lymphocytes. *J. Toxicol. Environ. Health Part A* **2021**, *85*, 353–363. [CrossRef] [PubMed]
52. Kim, M.; Yin, J.; Hwang, I.H.; Park, D.H.; Lee, E.K.; Kim, M.J.; Lee, M.W. Anti-Acne Vulgaris Effects of Pedunculagin from the Leaves of *Quercus Mongolica* by Anti-Inflammatory Activity and 5α-Reductase Inhibition. *Molecules* **2020**, *25*, 2154. [CrossRef] [PubMed]
53. Al-Harbi, R.; Al-Wegaisi, R.; Moharram, F.A.; Shaaban, M.; El-Rahman, O.A. Antibacterial and Antihemolytic Activity of Tannins from *Pimenta Dioica* against Methicillin Resistant *Staphylococcus Aureus*. *Bangladesh J. Pharmacol.* **2017**, *12*, 63–68. [CrossRef]
54. Hayashi, T.; Maruyama, H.; Kasai, R.; Hattori, K.; Takasuga, S.; Hazeki, O.; Yamasaki, K.; Tanaka, T. Ellagitannins from *Lagerstroemia Speciosa* as Activators of Glucose Transport in Fat Cells. *Planta Medica* **2002**, *68*, 173–175. [CrossRef] [PubMed]
55. Kantapan, J.; Dechsupa, N.; Tippanya, D.; Nobnop, W.; Chitapanarux, I. Gallotannin from *Bouea macrophylla* seed extract suppresses cancer stem-like cells and radiosensitizes head and neck cancer. *Int. J. Mol. Sci.* **2021**, *22*, 9253. [CrossRef]
56. Frisch, M.J.; Trucks, G.W.; Schlegel, H.B.; Scuseria, G.E.; Robb, M.A.; Cheeseman, J.R.; Scalmani, G.; Barone, V.; Petersson, G.A.; Nakatsuji, H.; et al. *Gaussian 16, Revision A.03*; Gaussian Inc.: Wallingford, CT, USA, 2016.

57. Tomasi, J.; Mennucci, B.; Cammi, R. Quantum mechanical continuum solvation models. *Chem. Rev.* **2005**, *105*, 2999–3094. [CrossRef] [PubMed]
58. Runge, E.; Gross, E.K. Density-functional theory for time-dependent systems. *Phys. Rev. Lett.* **1984**, *52*, 997. [CrossRef]
59. El-Zohry, A.M.; Orabi, E.A.; Karlsson, M.; Zietz, B. Twisted Intramolecular Charge Transfer (TICT) Controlled by Dimerization: An Overlooked Piece of the TICT Puzzle. *J. Phys. Chem. A* **2021**, *125*, 2885–2894. [CrossRef]